

Computational Modeling and Clonogenic Assay for Radioenhancement of Gold Nanoparticles Using 3D Live Cell Images

Author(s): Wonmo Sung, Yoon Jeong, Hyejin Kim, Hoibin Jeong, Clemens Grassberger, Seongmoon Jung, G-One Ahn, Il Han Kim, Jan Schuemann, Kangwon Lee and Sung-Joon Ye

Source: Radiation Research, 190(5):558-564.

Published By: Radiation Research Society

<https://doi.org/10.1667/RR15134.1>

URL: <http://www.bioone.org/doi/full/10.1667/RR15134.1>

BioOne (www.bioone.org) is a nonprofit, online aggregation of core research in the biological, ecological, and environmental sciences. BioOne provides a sustainable online platform for over 170 journals and books published by nonprofit societies, associations, museums, institutions, and presses.

Your use of this PDF, the BioOne Web site, and all posted and associated content indicates your acceptance of BioOne's Terms of Use, available at www.bioone.org/page/terms_of_use.

Usage of BioOne content is strictly limited to personal, educational, and non-commercial use. Commercial inquiries or rights and permissions requests should be directed to the individual publisher as copyright holder.

Computational Modeling and Clonogenic Assay for Radioenhancement of Gold Nanoparticles Using 3D Live Cell Images

Wonmo Sung,^a Yoon Jeong,^b Hyejin Kim,^a Hoibin Jeong,^d Clemens Grassberger,^e Seongmoon Jung,^a G-One Ahn,^d Il Han Kim,^{a,c} Jan Schuemann,^e Kangwon Lee^b and Sung-Joon Ye^{a,c,f,1}

Programs in ^a Biomedical Radiation Sciences and ^b Nano Science and Technology, Department of Transdisciplinary Studies, Graduate School of Convergence Science and Technology, and ^c Department of Radiation Oncology, Seoul National University College of Medicine, Seoul, Korea; ^d Division of Integrative Biosciences and Biotechnology, Pohang University of Science and Technology, Pohang, Korea; ^e Department of Radiation Oncology, Massachusetts General Hospital and Harvard Medical School, Boston, Massachusetts; and ^f Robotics Research Laboratory for Extreme Environment, Advanced Institutes of Convergence Technology, Seoul National University, Suwon, Korea

Sung, W., Jeong, Y., Kim, H., Jeong, H., Grassberger, C., Jung, S., Ahn, G-O., Kim, I. H., Schuemann, J., Lee, K. L. and Ye, S-J. Computational Modeling and Clonogenic Assay for Radioenhancement of Gold Nanoparticles Using 3D Live Cell Images. *Radiat. Res.* **190**, 558–564 (2018).

Radioenhancement of gold nanoparticles (GNPs) has shown great potential for increasing the therapeutic efficiency of radiotherapy. Here we report on a computational model of radiation response, which was developed to predict the survival curves of breast cancer cells incubated with GNPs. The amount of GNP uptake was estimated using inductively coupled plasma-mass spectroscopy, and the three-dimensional (3D) intracellular distribution of GNPs was obtained using optical diffraction tomography. The developed computational model utilized the 3D live cell imaging and recent Monte Carlo techniques to calculate microscopic dose distributions within the cell. Clonogenic assays with and without GNPs were performed to estimate the radioenhancement for 150 kVp X rays in terms of cell survival fractions. Measured cell survival fractions were comparable with the computational model. © 2018 by Radiation Research Society

INTRODUCTION

The goal of radiotherapy in cancer treatment is to maximize tumor cell death, while minimizing damage to healthy tissues. For the last two decades, advances in radiotherapy have been driven, in large part, by the delivery of improved physical dose distributions using intensity modulated radiation therapy (IMRT) and volumetric modulated radiation therapy (VMAT), in addition to other technical advances. The introduction of gold

nanoparticles (GNPs) into cancer cells has been shown to enhance the effect of radiation in the cells, further improving its therapeutic potential. This GNP-mediated radioenhancement was first demonstrated *in vivo* in mice bearing malignant tumors that received kV photon irradiation and intravenously injected GNPs (1). Subsequent *in vivo* and *in vitro* studies have further proved the effectiveness of GNP radioenhancement in irradiated animals and cells (2–5). This is attributed to the high photoelectric interaction probability of gold and therefore, the delivery of additional energy directly into cancer cells.

In initial efforts to explain GNP radioenhancement, macroscopic dose models were used. However, experimentally required concentrations of GNP to produce an observable effect were much less than those models predicted theoretically (2, 4, 6). Instead, the increased biological effectiveness was attributed to the heterogeneous dose deposition at the subcellular scale, the so called “microscopic dose” (7–11). The local effect model (LEM) was adapted to translate the microscopic dose enhancement to predict cell survival with GNPs (GNP-LEM) (11). Although theoretical studies based on GNP-LEM have revealed the importance of GNP distributions and cell geometry (12, 13), the geometric representations in these studies were overly simplified.

To visualize cell geometry and GNP distributions, various types of imaging techniques have been used. Transmission electron microscopy (TEM) is one of the standard high-resolution two-dimensional (2D) imaging tools but TEM requires cells to be fixated (i.e., dead) due to the vacuum environment for the high-intensity electron beam (14). Fluorescence imaging such as confocal microscopy can be implemented for this purpose, but fluorescent probes may alter the physiological properties of cells and require long acquisition time for three-dimensional (3D) imaging (15, 16). A recently published study presented a label-free method to measure 3D spatial distributions of GNPs inside

¹ Address for correspondence: Biomedical Radiation Sciences, Transdisciplinary Studies, Seoul National University, 2nd floor, 18-Dong, Gwanak-ro 1, Gwanak-gu, Seoul 08836, Republic of Korea; email: sye@snu.ac.kr.

live cells by employing optical diffraction tomography (ODT) (17, 18). This technology utilizes the refractive index as imaging contrast.

In this study, we used 3D distributions of GNPs in live cells as observed by ODT as input for our GNP radio-enhancement model. The microscopic dose distribution around a single GNP was calculated using Monte Carlo simulations. This radial dose distribution was then applied to the GNP-LEM, using the cell images to predict the dose dependence of cell survival and was then compared to experimental results.

MATERIALS AND METHODS

Optical Diffraction Tomography Images

The human breast cancer cells (MDA-MB-231) were maintained in Roswell Park Memorial Institute medium 1640 (RPMI-1640) supplemented with 10% fetal bovine serum and 1% penicillin/streptomycin and incubated for 24 h. The cells were maintained in a tissue culture incubator at 37°C and 5% CO₂/95% air. Spherical GNPs of 1.9 nm diameter, coated with a glucose derivative, were obtained from Nanoprobes Inc. (Yaphank, NY). GNPs were suspended in media and filtered through a 0.2-μm filter according to manufacturer instructions. The cells were treated with 500 μg/ml of 1.9-nm GNPs and incubated for 24 h.

Using a commercial ODT (HT-1H; Tomocube Inc., Daejeon, Korea), 3D intracellular localization of GNPs inside the cells was quantified using their high-refractive-index (RI) values. Cells were plated for 24 h, exposed to GNPs for another 24 h, washed three times in PBS and covered with a slide glass for ODT imaging. The control cells without GNP treatment were also prepared for ODT imaging. Image reconstruction was performed using commercial software (TomoStudio; Tomocube, Inc.). According to the manufacturer, the reconstructed spatial resolution of ODT is 110 nm laterally and 220 nm axially. The single-cell imaging was applicable in ODT as described elsewhere (19, 20). Currently, the ODT is somewhat limited due to multiple scattering in multilayered cells when acquiring a single-cell image. To acquire a single-cell image the region of interest was selected such that it contained only a single cell. These 3D images were then imported into an in-house software program in MATLAB® version 2016b (MathWorks® Inc., Natick, MA) for image segmentation. The cell membrane was detected by differences in RI from the background image. The cell membrane could be segmented by calculating image gradients, filling interior gaps and removing connected objects on the border. The cell nucleus was segmented manually. To determine the RI values of GNPs, average RI histograms for the GNP-treated and control cells were compared.

GNP Uptake

The GNP uptake assessment was also prepared with the same conditions as above and performed using inductively coupled plasma-mass spectrometry (ICP-MS). The cells were plated and treated with GNPs for 24 h, washed three times in phosphate buffered saline (PBS), trypsinized before counting and then digested in aqua regia. The sample was ionized by inductively-coupled plasma. Using the mass spectrometer, the gold ions were separated by their mass-to-charge ratio and a detector then received a signal proportional to the gold concentration in the sample. The gold content was determined using PerkinElmer® SCIEX NexION® 350D (Shelton, CT), which has a low detection limit at the parts per billion (ppb) range.

Clonogenic Assay

Control cells (without GNPs) were X-ray irradiated (150 kVp, 2-mm aluminum filter) using the X-RAD 320 (Precision X-Ray Inc., North Branford, CT). After irradiation, the cells were incubated for 14 days and media was changed during the incubation every 7 days. The resulting cell colonies were stained with crystal violet (0.5% weight/volume concentration) and counted. Survival fractions were then calculated relative to nonirradiated cells.

To verify the developed GNP-LEM prediction, clonogenic assay was performed for cells exposed to the same concentration (500 μg/ml) of GNPs. They were incubated for 24 h, irradiated and incubated for 2 weeks. The resulting cell colonies were stained and counted. Survival fractions were then calculated relative to nonirradiated cells. Using the clonogenic survival assays, colony formation in cells exposed to GNPs for 24 h was reduced by 21%. This was comparable to the 19.4% reduction reported in the literature (2).

Dosimetry Calculations

Monte Carlo simulations were performed to calculate nanoscale doses in the vicinity of single GNPs using the TOol for PArticle Simulation (TOPAS and the nanometer-scale extension TOPAS-nBio) (21–23). We have previously described the simulation details elsewhere (8, 12, 13). The spectra of a 150 kVp polychromatic X-ray beam (with a 2-mm aluminum filter) were acquired using SpekCalc 1.1 (24) and assumed to be based on a cylindrical water phantom. The phase space files were acquired at 1-mm depth in the phantom to reflect the experimental condition. The radius of the phase space was adjusted to have the same diameter as a single GNP (i.e., 1.9 nm). This phase space file was then used to irradiate a single GNP. The second phase space file was recorded on the GNP surface to score outgoing electrons. This second phase space was used as a source at the center of a cell-size water phantom. The radial dose distribution was calculated in spherical shells of 1-nm thickness around the source.

Effect Modeling

For radioenhancement modeling, the radial dose distribution was applied to 3D ODT images of the GNP distribution in a MDA-MB-231 cell. Each segmented voxel with RI > 1.38 in the image was considered as a cluster of GNP point sources. Assuming a constant GNP concentration across the cell, the number of GNPs per voxel was calculated by dividing the number of GNPs per cell by the total number of segmented voxels with RI > 1.38 in the images. The radial dose per ionization around the single GNP calculated by Monte Carlo simulations was superimposed and multiplied by the number of GNPs for each voxel and the interaction probability. This then provided a microscopic dose distribution throughout the 3D RI cell image, which was used as an input to the GNP-LEM procedure.

The dependence of cell survival on doses was estimated using the GNP-LEM, as described in our previously published work (12, 13). The basic assumption of the (GNP-)LEM is that the biological effect of radiation is determined by the spatial lethal event distributions inside the cell nucleus (25). The lethal events of each voxel in the cell nucleus were calculated from the determined doses to the nucleus regions. The lethal events (N) can be described using the X-ray dose-response curve (S_x) with a threshold dose D_t and a maximum slope $S_{max} = \alpha + \beta D_t$, which is given in Eq. (1):

$$N(D) = -\ln(S_x) = \begin{cases} -\ln(e^{-\alpha D - \beta D^2}) & (D \leq D_t) \\ -\ln(e^{-\alpha D_t - \beta D_t^2} e^{-S_{max}(D-D_t)}) & (D > D_t) \end{cases} \quad (1)$$

This two-way representation is due to overestimation of the linear-quadratic model in the high-dose region (26). The threshold dose D_t was set to 20 Gy, as reported elsewhere (27). The average number of lethal events (N) in the cell nucleus determines the macroscopic

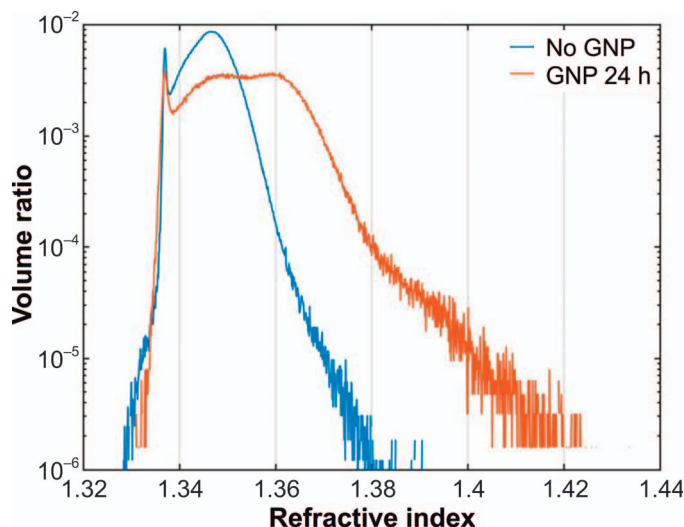


FIG. 1. Refractive index histograms without (i.e., noGNP) and with gold nanoparticles after 24 h exposure (GNP24h).

survival fraction with GNPs, as follows:

$$S_{GNP}(D) = e^{-\overline{N}(D)}. \quad (2)$$

RESULTS

Optical Diffraction Tomography Images

The 3D RI tomograms of GNP-treated and -untreated cells were observed using ODT. To determine the RI values of GNPs, average RI histograms of GNP-treated and control cells are shown together for comparison in Fig. 1. In the range of RI values higher than 1.38, a larger number of counts was observed in the GNP-treated cells compared to the control cells. Since it has been reported that the RI values of the cell cytoplasm is in the range of 1.37–1.39 (17), the range of RI values higher than the values of cytoplasm was assumed to correspond to GNPs.

The intracellular localization of GNPs was assumed to be in the regions where the RI values were higher than those of the normal cytoplasm (>1.38) (Fig. 2). Large amounts of aggregated GNPs were internalized into the cell, i.e., in cytoplasmic lysosomes and these aggregated GNPs were dispersed in the cytoplasm.

GNP Uptake

The number of GNPs per cell was calculated from the total mass of gold per sample as determined by ICP-MS using the method described by Coulter *et al.* (28). The concentration of gold element in a sample exposed to 500 $\mu\text{g/ml}$ GNPs was $1.47 \pm 0.02 \mu\text{g/ml}$. The number of cells per sample was 6.6×10^5 and the volume of the solution was 1 ml per sample. Assuming that a single GNP of 1.9-nm diameter contains approximately 200 gold atoms (29), the calculated average number of GNPs per cell was $3.40 \pm 0.04 \times 10^7$. Assuming the number of GNPs per cell is

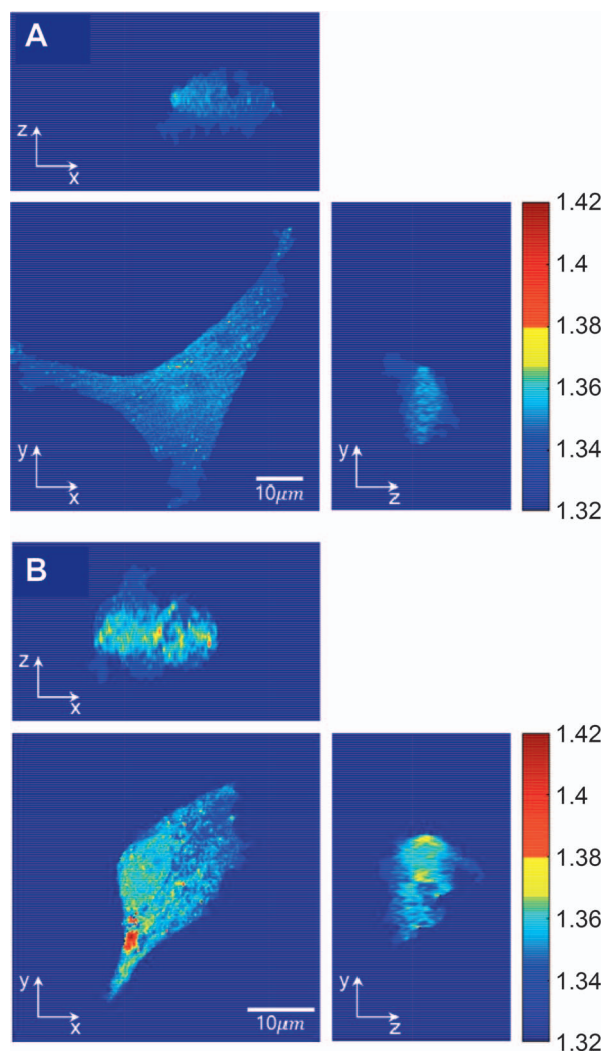


FIG. 2. Cross-sectional slices of 3D refractive index tomograms of MDA-MB-231 human breast cancer cells after 24 h treatment (panel A) without and (panel B) with GNPs. The values on the color bar indicate refractive indices.

constant across the cells, these values were used to determine the number of GNPs per voxels in ODT cell images and for GNP-LEM calculations.

Clonogenic Assay Without GNP

The radiation dose-response curve for MDA-MB-231 cells exposed to 150 kVp X rays was measured for α - and β -input parameters (Fig. 3). The curve was fitted with a simple linear-quadratic model, $survival\ fraction = e^{-\alpha D - \beta D^2}$, applying the nonlinear least-square method with and without weighted standard deviations. Optimization constraints were applied to force α and β values to be non-negative. This yielded radiation-response parameters of $\alpha = 0.020$, $\beta = 0.059$ and $\alpha = 2.2865 \times 10^{-6}$, $\beta = 0.0638$ without and with weighted standard deviations, respectively. The first set of data is nearly identical to values obtained by Jain *et al.* (2). For GNP-LEM prediction modeling, these values were used in Eq. (1) for the X-ray dose response without GNPs.

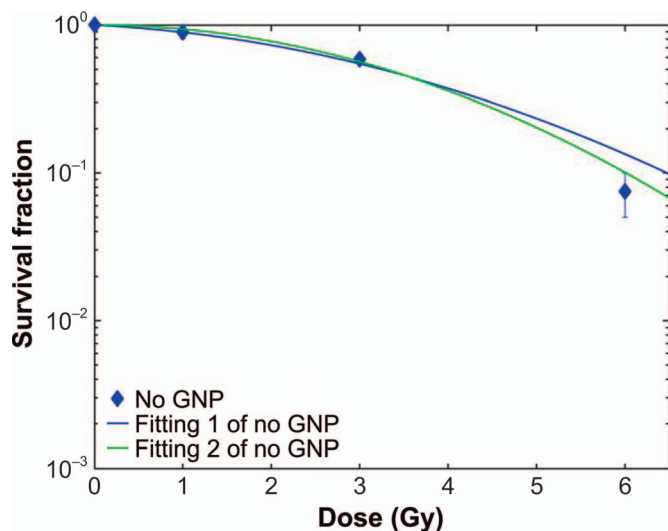


FIG. 3. Radiation dose-response data for MDA-MB-231 cells, without gold nanoparticles (GNPs), which were exposed to 1, 3 and 6 Gy of 150 kVp X rays. The solid lines indicate the fitting curve of cells not exposed to GNPs using a simple linear quadratic model [blue and green solid line for fitting without (Fitting 1) and with (Fitting 2) weighted standard deviations, respectively]. Error bars are one standard deviation at each corresponding dose-survival fraction point.

Dosimetry Calculations

From the Monte Carlo simulations, the interaction probability was determined to be 4.0×10^{-6} interactions per Gy per GNP. As shown in Fig. 4, the calculated dose distributions rapidly fell off within short distances from the surface of the GNP (<1% of the surface dose at 100 nm). Consequently, the GNPs induced microscopic dose spikes in close proximity to their surface during irradiation, leading to highly-heterogeneous dose distributions at the subcellular scale.

Effect Modeling

Assuming that ODT image voxels with RI values higher than 1.38 contained the number of GNPs per cell measured by ICP-MS, the number of GNPs per voxel was calculated for each 3D cell image. The doses around a single GNP were superimposed at each of the GNP locations on the 3D cell images (Fig. 5). The cell nucleus was manually identified as the region where lethal events can occur for GNP-LEM prediction.

Cellular GNP distributions were obtained from 3D images of five cells observed using the ODT method. Combining these GNP distributions into GNP-LEM, two cell survival predictions are shown in Fig. 6 along with experimental results. The error bars for the GNP-LEM indicate the variation due to the different intracellular GNP distributions. This indicates that the microscopic dose peaks in close proximity to GNPs can explain experimentally observed GNP dose enhancement. In addition, GNP-LEM predictions depend somewhat on the LQ model fitting parameters determined from the survival curves without GNPs.

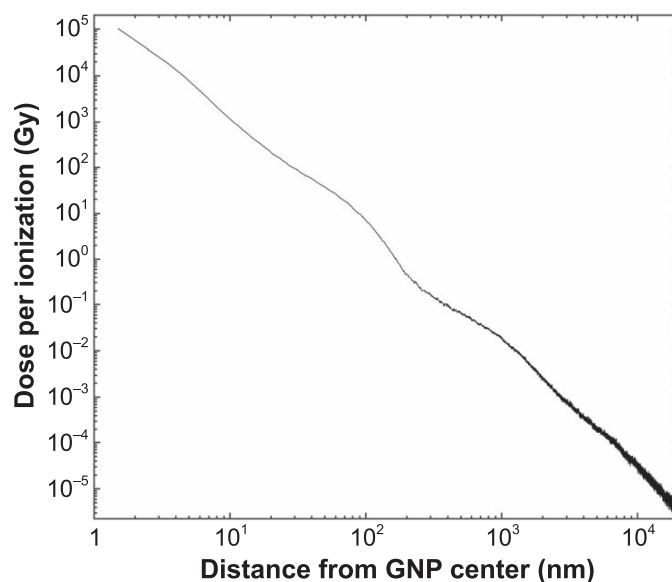


FIG. 4. Radial dose distribution per single ionizing event from a 1.9-nm GNP for 150 kVp X-ray irradiation.

The radiosensitization is often expressed in terms of sensitizer enhancement ratio (SER) (2, 30). The SER is defined as the ratio of the area under the survival curve of unirradiated cells and that of gold-exposed cells. MDA-MB-231 cells treated with GNPs and then exposed to 150 kVp X rays show significant radiosensitization with a SER of 1.34. The survival fraction of the control group at 6 Gy was 0.0750 while the corresponding value of cells exposed to GNPs for 24 h was 0.0214 at the same radiation dose.

DISCUSSION

The previously reported ODT development study confirmed that regions having high RI values correlate with the presence of GNPs by comparing confocal fluorescent images of the same cells with PEGylated GNPs (17). In this study it was assumed that any voxels with RI values higher than 1.38 contain GNPs. It is likely that the RI is indeed a measure for the localization and density of GNPs, with higher RI values indicating a larger number of GNPs. Nevertheless, this study assumes that all voxels with RI values higher than 1.38 have the same number of GNPs per voxel. Other techniques such as fluorescence imaging are necessary to obtain quantitative correlations of RI values and GNP concentration in ODT imaging. However, we postulate that the average number of GNPs per pixel determined in this study still provides a realistic distribution of GNPs that can be used to determine the microscopic dose distributions inside the cell. This study serves as a proof of principle to obtain GNP distributions in live cells.

The LEM model was originally developed to predict the enhanced biological effect of high-linear energy transfer (LET) radiation such as carbon-ion treatments using heterogeneous subcellular energy deposition (31). Like the

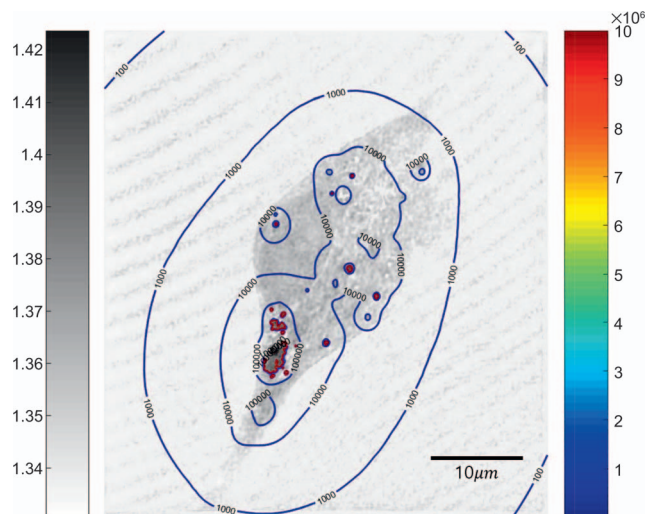


FIG. 5. Microscopic dose distributions on the cell image acquired by optical diffraction tomography. Grayscale: refractive index; color scale: microscopic dose (Gy/ionization).

halo of secondary electrons around the particle track for high-LET radiation, the secondary radiation emitted from GNPs includes a large number of short-range electrons. The GNP-LEM assumes that the highly-localized energy deposition by GNPs resembles the dose pattern deposited by high-LET radiations (32). In this study, GNP-LEM was applied to 3D live cell images and GNP uptake of MDA-MB-231 breast cancer cells. The GNP-LEM-predicted survival was comparable to experimental cell survival data.

The previously reported GNP-LEM studies have been developed with overly simplified 2D cell models based on TEM images (11–13). Those studies simply assumed cylinder shapes of the cell membranes and nucleus, which restricted GNP locations to a 2D space. Moreover, TEM requires pretreatment to fix the cell (i.e., using dead cells). However, 3D images of live cell structures acquired by ODT can provide a more realistic base for computational models to understand GNP radioenhancement.

For the current study, MDA-MB-231 breast cancer cell lines were chosen because they comprise radiation- and drug-resistant malignant tumors. Moreover, the fact that breast cancer is located underneath the skin makes it an attractive candidate for relatively high radioenhancement by GNPs using kilovoltage X rays. It has been previously reported that, *in vivo*, a GNP concentration ratio of tumor to normal tissue of approximately 8:1 was achieved (1). However, further studies are warranted to investigate GNP effects on normal epithelial cells for a successful clinical translation of GNP as a radiosensitizer. It is also important to note that the imaged GNP distributions and enhancement observed in this study may not directly translate to preclinical or clinical applications due to potential changes in various physiological and microenvironmental factors between *in vitro* and *in vivo* conditions. Nevertheless, live 3D images of cell structures acquired by ODT will still provide better representation of irradiated targets, thereby

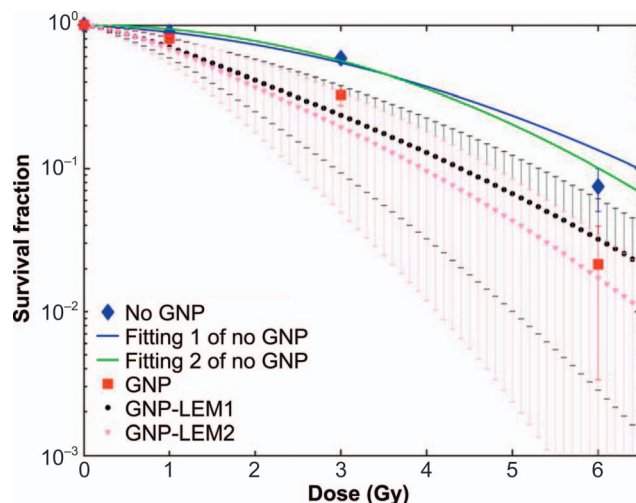


FIG. 6. Experimentally observed cell survival for MDA-MD-231 cells that were exposed to 1, 3 and 6 Gy of 150 kVp X rays (red square = with GNP; blue diamond = without GNP). Cell survival fitting without GNPs (blue and green solid line, 1: without and 2: with weighted standard deviation, respectively) and theoretically predicted with GNPs (brown and pink circles, derived from fitting with no GNPs, 1: without and 2: with weighted standard deviation, respectively). Error bars are one standard deviation at each corresponding dose-survival fraction point.

improving our understanding of radiation interactions with biological targets. Recently, temporal, fluorescence and *in vivo* imaging capabilities have been included within the ODT platform; such a combined imaging option could offer additional insights into the distribution and effects of GNPs in cells (33–35).

It is evident that the approach presented in this study predicted the observed sensitizing effects of colony formation after two weeks. Although GNP-LEM provides the macroscopic end point of biological cell survival, it cannot explain a comprehensive mechanism of GNP radioenhancement. Recently published studies suggested that in addition to the DNA in the nucleus, other damaged organelles such as mitochondria may play a role in cell killing related to GNP radioenhancement (36–38). Furthermore, a larger number of reactive oxygen species generated on the GNP surface may cause an elevated level of oxidative stress, which may damage the cell (39). However, the current approach, using 3D live cell imaging and Monte Carlo calculated microscopic dose distributions, offers a conceivable avenue to explain the GNP radioenhancement mechanisms.

CONCLUSIONS

A computational model of radiation response using 3D images of live breast cancer cells and the GNP uptake within these cells has shown good agreement with the experimental *in vitro* cell survival data. Contrary to the previous 2D modeling, with its overly simplified cellular structures and GNP uptakes, the 3D cell image-based

modeling, combined with Monte Carlo-calculated microdoses, can provide realistic cell survival predictions for the GNP radioenhancement.

ACKNOWLEDGMENTS

This work was supported in part by the National Research Foundation of Korea (NRF), which is funded by the Korean government's Ministry of Science, ICT and Future Planning (MSIP) (grant nos. NRF-2013 M2B2B1075776 and NRF-2013 M2B2B1075772). This research was also supported in part by the Bio & Medical Technology Development Program of the NRF, which is funded by the MSIP (grant no. NRF-2016M3A9B4919711). Further support for this work was provided in part by the National Institutes of Health/National Cancer Institute (NIH/NCI grant no. R01CA187003; "TOPAS-nBio: a Monte Carlo tool for radiation biology research"). We also thank Stephen McMahon for helpful discussion.

Received: May 10, 2018; accepted: August 9, 2018; published online: August 24, 2018

REFERENCES

- Hainfeld JF, Slatkin DN, Smilowitz HM. The use of gold nanoparticles to enhance radiotherapy in mice. *Phys Med Biol* 2004; 49:N309–15.
- Jain S, Coulter JA, Hounsell AR, Butterworth KT, McMahon SJ, Hyland WB, et al. Cell-specific radiosensitization by gold nanoparticles at megavoltage radiation energies. *Int J Radiat Oncol Biol Phys* 2011; 79:531–9.
- Hainfeld JF, Dilmanian FA, Zhong Z, Slatkin DN, Kalef-Ezra JA, Smilowitz HM. Gold nanoparticles enhance the radiation therapy of a murine squamous cell carcinoma. *Phys Med Biol* 2010; 55:3045–59.
- Rahman WN, Bishara N, Ackerly T, He CF, Jackson P, Wong C, et al. Enhancement of radiation effects by gold nanoparticles for superficial radiation therapy. *Nanomedicine* 2009; 5:136–42.
- Kunjachan S, Detappe A, Kumar R, Ireland T, Cameron L, Biancur DE, et al. Nanoparticle mediated tumor vascular disruption: a novel strategy in radiation therapy. *Nano Lett* 2015; 15:7488–96.
- Cho SH. Estimation of tumour dose enhancement due to gold nanoparticles during typical radiation treatments: a preliminary Monte Carlo study. *Phys Med Biol* 2005; 50:N163–73.
- Lechtman E, Mashouf S, Chattopadhyay N, Keller BM, Lai P, Cai Z, et al. A Monte Carlo-based model of gold nanoparticle radiosensitization accounting for increased radiobiological effectiveness. *Phys Med Biol* 2013; 58:3075–87.
- Lin Y, McMahon SJ, Scarpelli M, Paganetti H, Schuemann J. Comparing gold nano-particle enhanced radiotherapy with protons, megavoltage photons and kilovoltage photons: a Monte Carlo simulation. *Phys Med Biol* 2014; 59:7675–89.
- Lin Y, Paganetti H, McMahon SJ, Schuemann J. Gold nanoparticle induced vasculature damage in radiotherapy: Comparing protons, megavoltage photons, and kilovoltage photons. *Med Phys* 2015; 42:5890–902.
- Sung W, Jung S, Ye SJ. Evaluation of the microscopic dose enhancement for nanoparticle-enhanced Auger therapy. *Phys Med Biol* 2016; 61:7522–35.
- McMahon SJ, Hyland WB, Muir MF, Coulter JA, Jain S, Butterworth KT, et al. Biological consequences of nanoscale energy deposition near irradiated heavy atom nanoparticles. *Sci Rep* 2011; 1:18.
- Lin Y, McMahon SJ, Paganetti H, Schuemann J. Biological modeling of gold nanoparticle enhanced radiotherapy for proton therapy. *Phys Med Biol* 2015; 60:4149–68.
- Sung W, Ye SJ, McNamara AL, McMahon SJ, Hainfeld J, Shin J, et al. Dependence of gold nanoparticle radiosensitization on cell geometry. *Nanoscale* 2017; 9:5843–53.
- Kourkoutis LF, Plitzko JM, Baumeister W. Electron microscopy of biological materials at the nanometer scale. *Annu Rev Mater Res* 2012; 42:33–58.
- Fei Y, Sun YS, Li Y, Lau K, Yu H, Chokhawala HA, et al. Fluorescent labeling agents change binding profiles of glycan-binding proteins. *Mol Biosyst* 2011; 7:3343–52.
- McQuaid HN, Muir MF, Taggart LE, McMahon SJ, Coulter JA, Hyland WB, et al. Imaging and radiation effects of gold nanoparticles in tumour cells. *Sci Rep* 2016; 6:19442.
- Kim D, Oh N, Kim K, Lee S, Pack CG, Park JH, et al. Label-free high-resolution 3-D imaging of gold nanoparticles inside live cells using optical diffraction tomography. *Methods* 2018; 136:160–7.
- Grassberger C, Dinkelborg P, McNamara A, Schuemann JP, McMahon SJ, Willers H, et al. Digital holographic microscopy for nanoscale dose calculation and assessing gold nanoparticle uptake in live cells. *Int J Radiat Oncol Biol Phys* 2016; 96:S169–70.
- Kim K, Yoon J, Shin S, Lee S, Yang S-A, Park Y. Optical diffraction tomography techniques for the study of cell pathophysiology. *J Biomed Photonics Eng* 2016; 2.
- Phillips KG, Jacques SL, McCarty OJ. Measurement of single cell refractive index, dry mass, volume, and density using a transillumination microscope. *Phys Rev Lett* 2012; 109:118105.
- Agostinelli S, Allison J, Amako Ka, Apostolakis J, Araujo H, Arce P, et al. GEANT4 – a simulation toolkit. *Nucl Instrum Methods Phys Res A* 2003; 506:250–303.
- Perl J, Shin J, Schumann J, Faddegon B, Paganetti H. TOPAS: an innovative proton Monte Carlo platform for research and clinical applications. *Med Phys* 2012; 39:6818–37.
- McNamara A, Geng C, Turner R, Mendez JR, Perl J, Held K, et al. Validation of the radiobiology toolkit TOPAS-nBio in simple DNA geometries. *Phys Med Biol* 2017; 33:207–15.
- Poludniowski G, Landry G, DeBlois F, Evans PM, Verhaegen F. SpekCalc: a program to calculate photon spectra from tungsten anode x-ray tubes. *Phys Med Biol* 2009; 54:N433–8.
- Katz R. The parameter-free track structure model of Scholz and Kraft for heavy-ion cross sections. *Radiat Res* 2003; 160:724–8.
- Astrahan M. Some implications of linear-quadratic-linear radiation dose-response with regard to hypofractionation. *Med Phys* 2008; 35:4161–72.
- Kramer M, Jakel O, Haberer T, Kraft G, Schardt D, Weber U. Treatment planning for heavy-ion radiotherapy: physical beam model and dose optimization. *Phys Med Biol* 2000; 45:3299–317.
- Coulter JA, Jain S, Butterworth KT, Taggart LE, Dickson GR, McMahon SJ, et al. Cell type-dependent uptake, localization, and cytotoxicity of 1.9 nm gold nanoparticles. *Int J Nanomedicine* 2012; 7:2673–85.
- Gu YJ, Cheng J, Lin CC, Lam YW, Cheng SH, Wong WT. Nuclear penetration of surface functionalized gold nanoparticles. *Toxicol Appl Pharmacol* 2009; 237:196–204.
- Concepts IQ. Dosimetry in radiobiology (Report No. 30). *J ICRU* 1979.
- Scholz M, Kraft G. Calculation of heavy ion inactivation probabilities based on track structure, x-ray sensitivity and target size. *Radiat Prot Dosimetry* 1994; 52:29–33.
- Schuemann J, Berbeco R, Chithrani DB, Cho SH, Kumar R, McMahon SJ, et al. Roadmap to clinical use of gold nanoparticles for radiation sensitization. *Int J Radiat Oncol Biol Phys* 2016; 94:189–205.
- Yu H, Lee P, Lee K, Jang J, Lim J, Jang W, et al. In vivo deep tissue imaging using wavefront shaping optical coherence tomography. *J Biomed Opt* 2016; 21:101406.
- Park Y. Correlative approaches in commercial quantitative phase microscopy (conference presentation). *Proc SPIE 10503, Quantitative Phase Imaging IV, 10503Y (15 March 2018)*. San Francisco:

- International Society for Optics and Photonics; 2018. (<https://bit.ly/2OImZyn>)
35. Kim K, Kim KS, Park H, Ye JC, Park Y. Real-time visualization of 3-D dynamic microscopic objects using optical diffraction tomography. *Opt Express* 2013; 21:32269–78.
 36. McNamara AL, Kam WW, Scales N, McMahon SJ, Bennett JW, Byrne HL, et al., Dose enhancement effects to the nucleus and mitochondria from gold nanoparticles in the cytosol. *Phys Med Biol* 2016; 61:5993–6010.
 37. Karatas OF, Sezgin E, Aydin O, Culha M. Interaction of gold nanoparticles with mitochondria. *Colloids Surf B Biointerfaces* 2009; 71:315–8.
 38. Ghita M, McMahon SJ, Taggart LE, Butterworth KT, Schettino G, Prise KM. A mechanistic study of gold nanoparticle radiosensitisation using targeted microbeam irradiation. *Sci Rep* 2017; 7:44752.
 39. Butterworth KT, Coulter JA, Jain S, Forker J, McMahon SJ, Schettino G, et al. Evaluation of cytotoxicity and radiation enhancement using 1.9 nm gold particles: potential application for cancer therapy. *Nanotechnology* 2010; 21:295101.